High-luminescence non-doped green OLEDs based on a 9,9-diarylfluorene-terminated 2,1,3-benzothiadiazole derivative†

Sung-Yu Ku,[a] Liang-Chen Chi,[a] Wen-Yi Hung,*[b] Shih-Wei Yang,[b] Tsung-Cheng Tsai,[b] Ken-Tsung Wong,*[a] Yu-Hung Chen[c] and Chih-I Wu[c]

Received 13th August 2008, Accepted 14th November 2008
First published as an Advance Article on the web 18th December 2008
DOI: 10.1039/b814082k

We have prepared a highly efficient non-doped green organic light-emitting diode (OLED) incorporating a novel 9,9-diarylfluorene-terminated 2,1,3-benzothiadiazole green emitter (**DFBTA**), which exhibits an excellent solid state photoluminescence quantum yield (81%), and new triaryldiamines (**DPAInT2**, **DPAInF**) with high hole mobility derived from rigid and coplanar cores. The optimal device: ITO/**DPAInT2**/**DPAInF**/TCTA/**DFBTA**/Alq3/LiF/Al displayed impressive device characteristics, including a maximum external quantum efficiency (η_{ext}) of 3.7% (12.9 cd A^{-1}) and a maximum brightness at 168 000 cd m^{-2}.

Introduction

Since tris(8-hydroxyquinolate) aluminum (Alq3) was first demonstrated for green organic light-emitting diodes (OLEDs) by Tang and Van Slyke,[1] many attempts have been made to improve upon its electroluminescence (EL). The main obstacle for the realization of OLED device applications is the organic material, which should ideally combine a high fluorescence quantum yield (if used as the emitter), suitable energy level alignment, high thermal stability, and good thin-film morphology. Only a limited number of materials meet these requirements for advanced commercial application. Among the functional materials used in multilayer OLEDs, the emitting layer usually comprises a suitable host doped with fluorescent or phosphorescent dyes to achieve high EL quantum efficiency. For example, green OLEDs incorporating host materials doped with fluorescent dyes exhibit promising EL efficiencies and have been studied extensively. The commonly used green dyes, such as coumarin,[2] quinacridone,[3] quinoline,[4] quinoxaline,[5] and carbazole derivatives,[6] all suffer from evident self-quenching fluorescence in their pristine thin films, meaning that these structures can only be exploited as dopants. Successful doping requires precise control over the dopant concentration, which can increase the production cost relative to that of systems employing non-doped organic emitting layers. The other limiting factor is the phase separation encountered in the host–guest mixture, rendering energy transfer ineffective.[7] To pave the way towards successful commercialization, highly efficient green fluorescent emitters for non-doped OLEDs are in great demand. In this regard, Saitoh *et al.*[8] and Antoniadis *et al.*[9] have demonstrated efficient non-doped green OLEDs exhibiting external quantum efficiencies (η_{ext}) of 3–4%. However, their current efficiencies (<9 cd A^{-1}) and power efficiencies (5 lm W^{-1}) left some space for further improvement. Recently, Lee and coworkers[10] demonstrated a non-doped green (EL λ_{max} = 511 nm) OLED device incorporating a dually functional material, phenyl-9-[8-(7,10-diphenylfluoranthenyl)]phenylcarbazole (TDPFPC), that displays an impressive current efficiency of 10.1 cd A^{-1} and a power efficiency of 12.1 lm W^{-1}. In this paper, we report a molecule that combines the electron-accepting characteristics of 2,1,3-benzothiadiazole with the high photoluminescence of fluorene as a green emitter, and its application in a non-doped green OLED device. Through judicious selection of suitable hole injection (HIL) and hole transporting (HTL) layers, this device exhibited an extremely high luminescence (168 000 cd m^{-2}) with a maximum external quantum efficiency (η_{ext}) of 3.7%, a current efficiency of up to 12.9 cd A^{-1}, and a power efficiency of 11 lm W^{-1}.

For efficient green emission, core chromophores such as coumarin, quinacridone, quinoline, quinoxaline, and carbazole are usually equipped with donor–acceptor (D–A) structural features along the main conjugated backbone. The D–A charge transfer enables the green emission to appear with high quantum yields in dilute solutions. Such intermolecular dipole interactions are, however, detrimental to the photoluminescence efficiency in the solid state, retarding their uses as solid state emitters in OLED devices. One feasible solution toward developing green emitters with strong solid state emissions is to prepare quasi-symmetrical molecules possessing suppressed molecular dipoles. The relatively narrow band gap required for green emission can be achieved through incorporation of a core chromophore having quinoid character. We selected 2,1,3-benzothiadiazole as the core structure for our green emitter because its derivatives possess excellent electro-optical properties, including high

[a]*Department of Chemistry, National Taiwan University, Taipei 106, Taiwan. E-mail: kenwong@ntu.edu.tw; Fax: +886 2 33661667; Tel: +886 2 33661665*
[b]*Institute of Optoelectronic Sciences, National Taiwan Ocean University, Keelung 202. E-mail: wenhung@mail.ntou.edu.tw; Fax: +886 2 24634360; Tel: +886 2 24622192 ext. 6718*
[c]*Department of Electrical Engineering and Graduate Institute of Photonic and Optoelectronic Engineering, National Taiwan University, Taipei 106, Taiwan*

† Electronic supplementary information (ESI) available: A comparion of EL spectra of devices III and IV to the PL of Alq3, device characteristics of using TAZ as ETL in device IV, UPS analysis of **DFBTA, DPAInT2** and **DPAInF**. See DOI: 10.1039/b814082k

fluorescence quantum yields and high electron affinities.[11] A commonly used strategy to acquire morphological stability without substantially altering the electro-optical properties of a core chromophore is to introduce bulky, rigid, and inert peripheral substituents that effectively suppress the tendency to crystallize. Along this line, we selected 9-biphenyl-9-tolylfluorene units as end-capping groups for the 2,1,3-benzothiadiazole core. In a previous study, we prepared bis(9,9-diarylfluorene) derivatives as efficient and stable UV-emitting materials;[12] the peripheral aryl groups connected to the C9 carbon atom of the fluorene unit contribute significantly to the improved thermal and morphological stability and high photoluminescence quantum yields. The two different aryl C9-substituents of the fluorene moiety, which are isolated from the main conjugation of the chromophore *via* an sp^3-hybridized carbon atom, suppress the tendency to crystallize and maintain the film's amorphous morphology. Through this design, the terminal bulky 9,9-diarylfluorene units prevent direct π–π stacking interactions of the active benzothiadiazole chromophores, thereby avoiding aggregation/self-quenching problems and maintaining the molecule's strong fluorescence in the solid state.

Results and discussion

Scheme 1 depicts the synthesis route for the green emitter 4,7-bis(9,9-diarylfluorenyl)–2,1,3-benzothiadiazole (**DFBTA**). The 9,9-diaryl-substituted 2-bromofluorene **1** was synthesized through the addition of biphenylmagnesium bromide to the corresponding 2-bromofluorenone, followed by a sulfuric acid-promoted Friedel–Crafts reaction (50% over two steps). The transformation of the bromide **1** into the corresponding pinacolato boronic ester **2** was achieved in good yield (78%) after lithiating compound **1** with an excess amount of *n*-BuLi at −78 °C and then treating the lithiated complex with 2-isopropoxy-4,4,5,5-tetramethyl-[1,3,2]dioxaborolane. Finally, Pd-catalyzed Suzuki coupling of the boronic ester **2** and 4,7-dibromo-benzo[1,2,5]thiadiazole was accomplished by adding a catalytic amount of tri-*tert*-butylphosphine as a promoter to afford the target **DFBTA** in moderate yield (60%).

Despite the interesting photoluminescence properties of benzothiadiazole-based molecules, the practical fabrication of high-efficiency OLEDs is seriously limited by the morphological stability and energy levels alignment of neighboring functional layers. Therefore, it was essential for us to develop contiguous materials that are compatible with **DFBTA** to improve the OLEDs' performances. Thus, we synthesized new diphenylamino group-terminated hole injection and transport materials. Diphenylamino moieties have been employed previously with fluorene-based oligomers to improve the hole injection and transporting properties of OLEDs, thereby enhancing the device efficiency and stability.[13] We developed our new hole injection and transport materials from rigid and coplanar cores in which *p*-tolyl substituents occupy the top and bottom faces of the main conjugated backbone. The introduction of aryl substituents prevented undesirable aggregation and improved the thermal and morphological stability, allowing the formation of homogeneous, stable amorphous films through thermal evaporation—a critical issue for the preparation of OLEDs.[14]

We derived the new hole injection material, the diphenylamino-terminated s-indaceno[1,2-b:5,6-b′]dithiophene **DPAInT2**, from an electron-rich coplanar s-indaceno[1,2-b:5,6-b′] dithiophene core structure. Scheme 2 depicts our synthesis route for **DPAInT2**. We have previously reported the synthesis of the coplanar core **3**[14b] featuring two fused thiophene rings. Selective bromination of **3** with 2 eq. of NBS afforded the dibromide **4** in 83%. Pd-catalyzed C–N bond cross-coupling of **4** with diphenylamine gave the desired product **DPAInT2** in 90% yield. We synthesized the new hole transporter, the diphenylamino-terminated indeno[1,2-b]fluorene **DPAInF**, through the selective bromination of the coplanar indeno[1,2-b]fluorene derivative **5**[14a] with 2.2 eq. of Br_2 in the presence of a catalytic amount of $FeCl_3$ (0.05 eq.) to afford the dibromo chromophore **6** in 95% yield. Pd-catalyzed C–N bond cross-coupling of **6** with diphenylamine gave the new hole-transporting material **DPAInF** in an isolated yield of 68%.

We used differential scanning calorimetry (DSC) and thermogravimetric analysis (TGA) to characterize the morphological and thermal properties, respectively, of the green emitter **DFBTA**, the hole injector **DPAInT2**, and the hole transporter

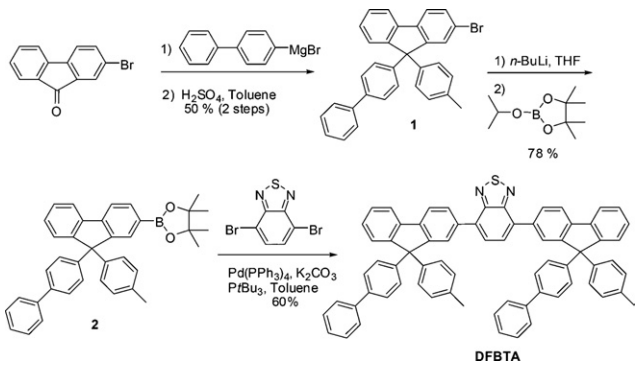

Scheme 1 The synthesis route for the green emitter **DFBTA**.

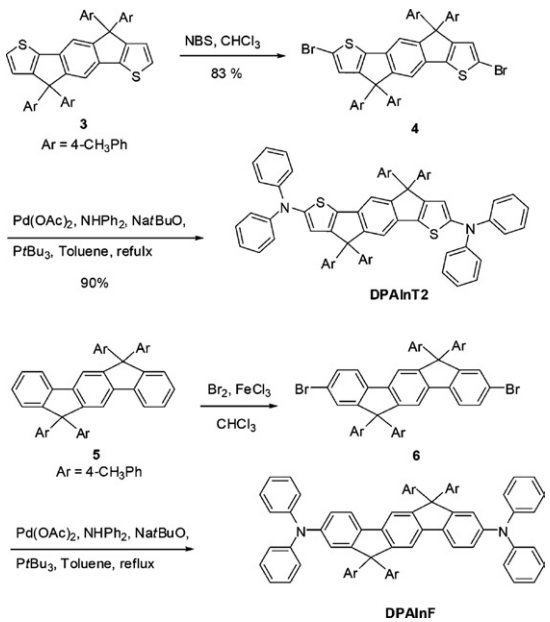

Scheme 2 The synthesis routes for the hole injector **DPAInT2** and the hole transporter **DPAInF**.

Table 1 Physical properties of the green emitter **DFBTA**, the hole injector **DPAInT2**, and the hole transporter **DPAInF**

Compound	T_g/°C	T_m/°C	T_d/°C	$E_{1/2}^{OX}$/V	$E_{1/2}^{REV}$/V	ΔE/mV[a]	HOMO/ eV[b]	LUMO/ eV[c]	ΔE_g/eV	Abs λ_{max}sol.; film/nm	PL λ_{max}sol.; film/nm
DFBTA	180	—	459	—	−1.29,−1.84	193,186	−6.40	−3.82	2.58	310,415; 315,421	525; 544
DPAInT2	176	—	418	0.47,0.60	—	100,94	−5.20	−2.58	2.62	412; 420	467,495; 470,503
DPAInF	183	390	420	0.75,0.95	—	100,100	−5.60	−2.68	2.92	405; 407	423,448; 427,452

[a] For each individual redox couple, $\Delta E = E_{pc} - E_{pa}$. [b] Determined by valence-band ultraviolet photoemission spectra (UPS) measurements. [c] LUMO = HOMO + ΔE_g, where ΔE_g was calculated from the absorption onset of solid film.

DPAInF; Table 1 summarizes the results. **DFBTA**, **DPAInT2**, and **DPAInF** exhibit distinct glass transition temperatures (T_g) higher than 150 °C; therefore, these materials can form homogeneous and stable amorphous films, an essential property for OLED device applications requiring thermal evaporation. We ascribe the amorphous behavior and high values of T_g to the rigidity of the conjugated backbones and the presence of the peripheral *p*-tolyl substituents, which effectively suppress intermolecular interactions. The aryl substituents also impart these materials with high tolerance toward thermal degradation, as indicated by their high decomposition temperatures (T_d).

We performed cyclic voltammetry to probe the electrochemical behavior of **DFBTA**, **DPAInT2**, and **DPAInF** (Fig. 1). **DPAInT2** and **DPAInF** feature two consecutive quasi reversible oxidation peaks, with those of the latter occurring at more positive oxidation potentials. We attribute the lower oxidation potentials of **DPAInT2** to the electron-donating character of the thiophene moieties embedded in its conjugated backbone. The green emitter **DFBTA** exhibits two quasi reversible reduction peaks at −1.29 and −1.84 V (*vs.* Ag/AgCl). We ascribe the first of these reduction peaks to the high electron affinity of the benzothiadiazole moiety; the distinct potential difference (550 mV) between the two reductions clearly reveals the excellent charge delocalization along the conjugated backbone of **DFBTA** upon incorporating the fluorene groups. Ultraviolet photoemission spectroscopy (UPS) was ultilized to unambiguiosly determine the ionization potentials of **DFBTA**, **DPAInT2**, and **DPAInF** in solid films (ESI).† On the basis of the UPS data and the optical band gaps, Table 1 summarizes the corresponding HOMO and LUMO energy levels of **DFBTA**, **DPAInT2** and **DPAInF**. The HOMO energy level of **DPAInT2**, which we estimated to be −5.20 eV, is close to the work function of ITO, indicating that it might feasibly behave as an effective hole-injection material and potentially serves as an alternative of the most popularly used hole injection layer, poly(3,4-ethylenedioxythiophene):poly(styrene sulfonate) (PEDOT:PSS).

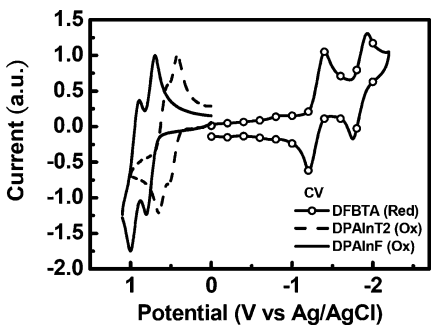

Fig. 1 Cyclic voltammograms of **DFBTA**, **DPAInT2**, and **DPAInF**.

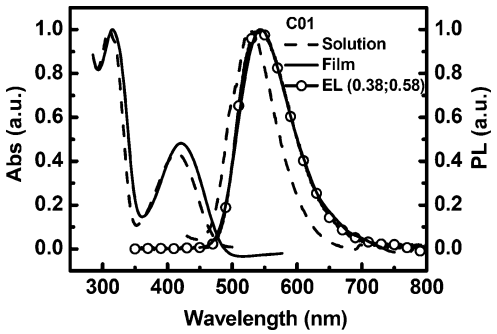

Fig. 2 UV–Vis absorption and photoluminescence (PL) spectra of **DFBTA** in dilute dichloromethane solution and as a solid film, and the electroluminescence (EL) spectrum of a device incorporating **DFBTA** as an emitter.

Fig. 2 indicates that the absorption and emission maxima of **DFBTA** in solid films are slightly red-shifted relative to those obtained in dilute solution; Table 1 summarizes the data. More importantly, the photoluminescence quantum yields of **DFBTA**, measured using a Hamamatsu C9920 integrating sphere, were very high: 81% as a thin film, 100% in solution.[15] These quantum yields are significantly higher than those of the prototypical green emitter Alq3 ($film_{PL}$: *ca.* 25%).[16] These results clearly indicate the effectiveness of introducing sterically bulky 9,9-diarylfluorene units as termini of a 2,1,3-benzothiadiazole core—evidently suppressing the detrimental intermolecular interactions and reducing the quenching processes.

We conducted charge-carrier mobility measurements of **DFBTA**, **DPAInT2**, and **DPAInF** using time-of-flight (TOF) techniques at ambient temperature.[17] The devices having the configuration glass/Ag (30 nm)/organic (2–3 μm)/Ag (150 nm) were prepared by vacuum deposition and then placed inside a cryostat and maintained under vacuum. Fig. 3(a) and (b) display typical room-temperature TOF transients of holes for **DPAInT2** and **DPAInF** under an applied electric field. The TOF transients reveal that **DPAInT2** exhibits dispersive hole-transporting behavior and **DPAInF** exhibits non- dispersive hole-transporting characteristics, respectively. In the double-logarithmic representations [insets to Fig. 3(a) and (b)], the carrier-transit time, t_T, required to determine the carrier mobilities, was extracted from the intersection point of the two asymptotes. The field dependence of the hole mobility, μ, was determined [Fig. 3(c)] from the transit time t_T according to the equation $\mu = d^2/Vt_T$, where d is the sample thickness and V is the

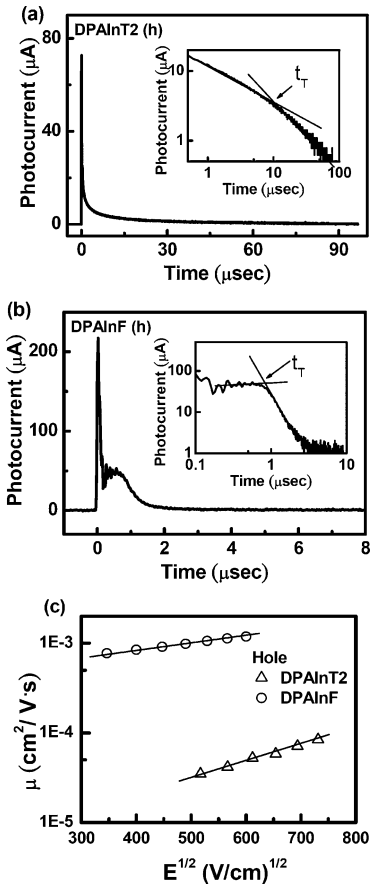

Fig. 3 TOF transients for holes: (a) **DPAInT2** (1.87 μm thick); $E = 3.75 \times 10^5$ V cm^{-1}; (b) **DPAInF** (2.55 μm thick); $E = 2.75 \times 10^5$ V cm^{-1}. Insets: double logarithmic plots of (a) and (b). (c) Hole mobilities plotted *versus* $E^{1/2}$.

applied voltage. The hole mobilities exist in the range 3×10^{-5} to 1×10^{-3} cm^2 V^{-1} s^{-1} for fields varying from 1.0 to 5.3 $\times$ 10^5 V cm^{-1}. The observed hole mobility in **DPAInT2** ($\mu_h = ca.\ 3 \times 10^{-5}$ cm^2 V^{-1} s^{-1}) is lower by approximately two orders of magnitude relative to that of its pure hydrocarbon counterpart, **DPAInF** ($\mu_h = ca.\ 1 \times 10^{-3}$ cm^2 V^{-1} s^{-1}) under the same electric field ($E = 2.8 \times 10^5$ V cm^{-1}). We ascribe the low mobility of **DPAInT2** mainly to the relatively nonlinear molecular backbone that originates from the intrinsic molecular geometry of the thiophene ring. This deviation from linearity for **DPAInT2** increases the complexity of its molecular ordering in solid films, rendering carrier transport more difficult. For **DFBTA**, the transient photocurrent signal was too weak to evaluate its mobility using the TOF technique.

To achieve high-efficiency OLEDs, it is necessary to feature an emitter having a high photoluminescence quantum efficiency (Φ_{PL}) in devices of sophisticated construction with judicious selections of compatible functional materials. Of primary importance in the device architecture are a small hole/electron injection barrier from the hole/electron transport layer to the emitting layer and a balanced current density of electrons and holes in the emitting layer, which will favor a low driving voltage and a high device efficiency. To evaluate the feasibility of using **DFBTA** as an emitting material, **DPAInT2** as a hole-injection material, and **DPAInF** as a hole-transporting material, we fabricated four different non-doped green-emitting devices (**I**–**IV**) having the structure ITO/HIL (20 nm)/HTL (20 nm)/TCTA (10 nm)/**DFBTA** (30 nm)/ETL (30 nm)/LiF (0.5 nm)/Al (150 nm) (Scheme 3). Here, PEDOT:PSS and **DPAInT2** were used as the HIL; 4,4′-bis[*N*-(1-naphthyl)-*N*-phenyl-amino]biphenyl (NPB) and **DPAInF** were used as the HTL. Insertion of a hole-transporting material 4,4′,4″-tris(*N*-carbazolyl)triphenylamine (TCTA) with the required energy levels between HTL and **DFBTA**, can reduce the hole-injection barrier to **DFBTA**. Alq3 was used in devices **II** and **IV** as the electron-transporting/hole-blocking layer. Lithium fluoride (LiF) was used as the electron-injection layer; aluminum (Al) was the cathode. Fig. 2 reveals that the electroluminescence (EL) spectra of these devices display no emissions from other materials (ESI†)—only the green-light emission from **DFBTA** with $CIE_{x,y}$ 1931 (Commission Internationale de L'Eclairage) coordinates of (0.38, 0.58).

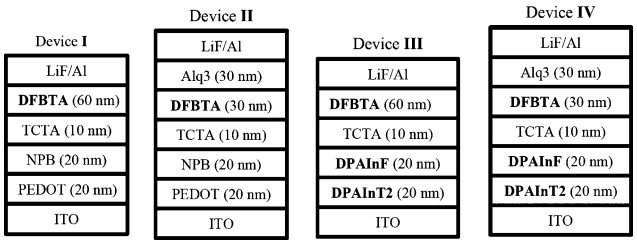

Scheme 3 Schematic structures of the four devices.

Fig. 4 and Table 2 provide the current–voltage–brightness (*I*–*V*–*L*) characteristics and EL efficiencies of the four devices. In device **I** we used conventional PEDOT:PSS and NPB as the HIL

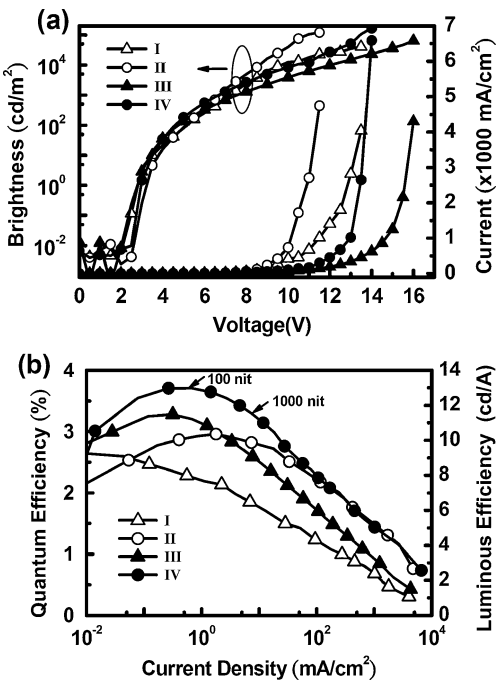

Fig. 4 Performances of devices I–IV: (a) current density–voltage–brightness (*I*–*V*–*L*) characteristics; (b) external quantum efficiency and luminance efficiency plotted with respect to current density.

Table 2 EL properties of devices **I–IV**

Device	I	II	III	IV
HIL/HTL	PEDOT:PSS/NPB	PEDOT:PSS/NPB	**DPAInT2/DPAInF**	**DPAInT2/DPAInF**
ETL	**DFBTA**	Alq3	**DFBTA**	Alq3
V_{on}/V	2	2.5	2	2.5
η (100 nit)/V; (%); /lm W^{-1}	5.1; 2.2; 4.5	4.7; 2.9; 5.9	5; 3.2; 7.5	4.6; 3.7; 8.5
L_{max}/cd m^{-2}; /V	40 700; 13.5	122 000; 11.5	64 000; 16	168 000; 14
I_{max}/mA cm^{-2}	4030	4750	4300	6600
$\eta_{ext,\ max}$ (%); /cd A^{-1}	2.6; 8.6	3; 10	3.3; 11.4	3.7; 12.9
$\eta_{p\ max}$/lm W^{-1}	9	7.7	11.2	11

and HTL, respectively; this device exhibited a maximum external quantum efficiency of 2.6% (8.6 cd A^{-1}). For comparison and optimization purposes, in device **III** we replaced the PEDOT:PSS and NPB with **DPAInT2** and **DPAInF**, respectively. The new HIL and HTL possess higher thermal stability and provide more-balanced carrier recombination in **DFBTA**. Accordingly, device **III** displayed enhanced EL performance relative to that of device **I**; the maximum external quantum efficiency of device **III** reached 3.3% (11.4 cd A^{-1}). In addition, the introduction of **DPAInT2** as the HIL offers a significant advantage over conventional PEDOT:PSS in that the pure organic HIL material does not produce acidity to etch ITO or introduce contamination into the HTL.[18] In devices **II** and **IV**, the insertion of Alq3 as the electron-transport layer between **DFBTA** and the cathode was crucial to block holes and to confine excitons within the emissive zone. As a consequence, devices **II** and **IV** exhibited lower driving voltages and higher performance relative to those of devices **I** and **III** (Table 2). The decreased driving voltage can be attributed to the low electron-injection barrier for Alq3 to enhance the current density of the device; for example, $J = 6600$ mA cm^{-2} in device **IV**. Among these four devices, device **IV** exhibited the highest efficiency: a turn-on voltage of 2.5 V (defined as the voltage at which the EL is rapidly enhanced), a maximum external quantum efficiency of 3.7% (12.9 cd A^{-1}) at 100 cd m^{-2}, and a low driving voltage of 4.6 V. As far as we are aware, this is the best performance reported to date for a non-doped green-light-emitting OLED. In addition, device **IV** possesses good durability, a high value of η_{ext} of 2.25% at 100 mA cm^{-2}, and a maximum luminance of 168 000 cd m^{-2} at 6600 mA cm^{-2} (14 V). Furthermore, replace the electron-transporting material in device **IV** from Alq3 to 3-(biphenyl-4-yl)-4-phenyl-5-(4-tert-butylphenyl)-1,2,4-triazole (TAZ) only led to device with lower maximum η_{ext} (3.13 %) as compared to that of the parent device (ESI).†

Conclusions

In summary, we have synthesized and characterized (i) a highly efficient green emitter (**DFBTA**) based on a 2,1,3-benzothiadiazole core terminated with bulky 9,9-diarylfluorene and (ii) two triaryldiamines (**DPAInT2**, **DPAInF**) derived from rigid and coplanar cores. The peripheral aryl substituents of these novel materials provide sufficient steric hindrance to mitigate intermolecular interactions, rendering these novel materials with high morphological and thermal stability, and high PL quantum yields for **DFBTA** in solid films (up to 81%). Combining the high PL efficiency of **DFBTA** (emitter), the high HOMO energy of **DPAInT2** (hole injection layer), and the high hole mobility of **DPAInF** (hole transport layer), we fabricated an optimal device having the configuration ITO/**DPAInT2/DPAInF**/TCTA/**DFBTA**/Alq3/LiF/Al that featured improved carrier injection and transport and good exciton confinement in the emissive layer. This device exhibited a maximum external quantum efficiency (η_{ext}) of 3.7% (12.9 cd A^{-1}), a maximum brightness of 168 000 cd m^{-2}, and good durability, as well as a high value of η_{ext} of 2.25% at a luminance of 8000 cd m^{-2} and a current density of 100 mA cm^{-2}.

Experimental

Synthesis of bromide 1

Under reflux, a suspension of the yellow solid 2-bromofluorenone (6.4 g, 25.0 mmol) in THF (100 mL) was added into a flask containing biphenylmagnesium bromide, which had been prepared in advance from 4-bromobiphenyl (8.7 g, 37.5 mmol) and magnesium (0.9 g, 37.5 mmol) in THF (100 mL). The mixture was heated under reflux for another 6 h and then cooled to room temperature, quenched with water, and extracted twice with EtOAc. The combined organic extracts were dried ($MgSO_4$) and concentrated by rotary evaporation. Recrystallization (CH_2Cl_2–hexane) afforded a crude product that was dissolved in toluene and added slowly into a mixture of toluene and concentrated H_2SO_4 (1 mL) under reflux; the resulting mixture was then heated under reflux with stirring for 6 h. The cooled solution was quenched with saturated aqueous $NaHCO_3$ and extracted twice with CH_2Cl_2. The combined organic solution was dried ($MgSO_4$) and concentrated under vacuum to yield **1** (6.1 g, 50%) as a white solid, which was purified by column chromatography (EtOAc–hexane, 1 : 3). M.p. 141−143 °C; ν_{max}(film)/cm^{-1} 3435, 3067, 3027, 2916, 2390, 1608, 1562, 1512, 1411, 1267, 1162, 1008, 813, 770, 731 cm^{-1}; ^{1}H NMR ($CDCl_3$, 400 MHz) δ 7.73 (1H, d, J 7.6, Ar–H), 7.63 (1H, d, J 8.0, Ar–H), 7.56–7.54 (2H, m, Ar–H), 7.53–7.46 (3H, m, Ar–H), 7.46–7.38 (6H, m, Ar–H), 7.36–7.30 (3H, m, Ar–H), 7.11 (2H, d, J 8.0, Ar–H), 7.07 (2H, d, J 8.0, Ar–H), 2.32 (3H, s, Ar–CH_3); ^{13}C NMR ($CDCl_3$, 100 MHz) δ 152.8, 150.5, 143.8, 141.6, 140.1, 139.2, 138.7, 138.5, 136.2, 130.3, 129.0, 128.7, 128.3, 128.0, 127.8, 127.6, 127.3, 126.8, 126.7, 126.6, 125.8, 121.2, 121.1, 119.9, 65.1, 21.4; MS (*m*/*z*, FAB$^+$) 488 (100), 486 (95); HRMS Calcd for $C_{32}H_{23}{}^{79}Br$ 486.0983, found 486.0982.

Synthesis of boronic ester 2

N-Butyllithium (1.6 M, 1.9 mL, 3.0 mmol) was added slowly into a flask containing compound **1** (974 mg, 2 mmol) in THF

(20 mL) at −78 °C and then the mixture was stirred at that temperature for 1 h. 2-Isopropoxy-4,4,5,5-tetramethyl[1,3,2]dioxaborolane (0.6 mL, 3.0 mmol) was added at −78 °C and then the mixture was warmed to room temperature slowly over a period of 6 h. The mixture was quenched with water and extracted twice with CH_2Cl_2. The combined organic phases were dried ($MgSO_4$) and concentrated in vacuo. The residue was purified by recrystallization (CH_2Cl_2/pentane) to yield **2** (833 mg, 78%) as a white solid. M.p. 137–140 °C; ν_{max}(film)/cm^{-1} 2970, 1593, 1490, 1352, 1142, 1075, 845, 732 cm^{-1}; ^{1}H NMR ($CDCl_3$, 400 MHz) δ 8.00 (1H, s, Ar–H), 7.95 (1H, d, *J* 7.6, Ar–H), 7.89–7.86 (2H, m, Ar–H), 7.62−7.60 (2H, m, Ar–H), 7.53−7.48 (3H, m, Ar–H), 7.46–7.41 (3H, m, Ar–H), 7.39–7.34 (4H, m, Ar–H), 7.34–7.23 (2H, m, Ar–H), 7.13 (1H, d, *J* 8.4, Ar–H), 2.37 (3H s, Ar–CH_3), 1.39 (12H, s, 4 × CH_3); ^{13}C NMR ($CDCl_3$, 100 MHz) δ 151.4, 150.7, 150.0, 144.5, 142.5, 142.1, 140.2, 139.3, 138.7, 135.6, 133.8, 131.7, 128.5, 128.2, 128.1, 127.7, 127.6, 127.3, 126.6, 126.5, 126.4, 125.8, 125.7, 120.2, 119.8, 119.1, 83.6, 64.9, 25.2, 21.3; MS (*m*/*z*, FAB$^+$) 534.2 (100); HRMS Calcd for $C_{38}H_{35}BO_2$ 534.2730, found 534.2755.

Synthesis of green emitter DFBTA

$Pd(PPh_3)_4$ (115 mg, 0.1 mmol), 4,7-dibromobenzo[1,2,5]thiadiazole (293 mg, 1.0 mmol), and 2-(9-biphenyl-9-tolylfluorene)pinacol boronate (1175 mg, 2.0 mmol) were placed into a 250 mL two-neck flask equipped with a septum. The flask was evacuated and back-filled with argon. Toluene (50 mL), K_2CO_3 (1.4 mL, 1.5 M, 2.1 mmol), and *t*Bu_3P (0.05 M in toluene, 2 mL, 0.1 mmol) were added to the flask *via* syringe at room temperature. After heating at 110 °C for 72 h, the reaction mixture was cooled to room temperature, water (80 mL) was added, and the mixture was extracted with CH_2Cl_2 (3 × 80 mL). The combined organic phases were dried ($MgSO_4$) and concentrated in vacuo to yield **DFBTA** (568 mg, 60%) as a yellow solid, which was purified through column chromatography ($CHCl_3$–toluene–hexane, 1 : 3 : 3). M.p. > 400 °C (DSC); ν_{max}(film)/cm^{-1} 3065, 3032, 1600, 1487, 1449, 1016, 731 cm^{-1}; ^{1}H NMR ($CDCl_3$, 400 MHz) δ 8.06 (2H, d, *J* 8.8, Ar–H), 7.97 (2H, s, Ar–H), 7.92 (2H, d, *J* 8.0, Ar–H), 7.83 (2H, d, *J* 7.2, Ar–H), 7.69 (2H, s, Ar–H), 7.52 (4 H, d, *J* 7.2, Ar–H), 7.84–7.27 (20H, m, Ar–H), 7.21 (4H, d, *J* 8.4, Ar–H), 7.06 (4H, d, *J* 8.4, Ar–H), 2.29 (6H, s, 2 × Ar–CH_3); ^{13}C NMR ($CDCl_3$, 100 MHz) δ 153.9, 151.5, 144.8, 142.5, 140.5, 140.2, 139.5, 139.2, 136.6, 136.1, 133.1, 128.8, 128.5, 128.0, 127.8, 127.7, 127.4, 126.9, 126.8, 126.1, 120.3, 120.0, 65.1, 21.0; MS (*m*/*z*, FAB$^+$) 949.5 (60), 391.3 (80), 307.0 (100); HRMS Calcd for $C_{70}H_{48}N_2S$ 948.3538, found 948.3953; Anal. Calcd for $C_{70}H_{48}N_2S$ C, 88.57, H 5.10, N, 2.95, found C, 88.58, H, 4.46, N, 2.84.

Synthesis of dibromide 4

Compound **3** (2.75 g, 4.37 mmol) was dissolved in $CHCl_3$ (100 mL) in a 250 mL flask wrapped in aluminum foil to protect the contents from light. NBS (1.56 g, 8.75 mmol) was added into the flask and the reaction mixture was stirred at 25 °C for 2 h. The mixture was partitioned between CH_2Cl_2 and water and then the organic phase was collected, dried ($MgSO_4$), and concentrated under rotary evaporation. The product was purified through recrystallization (CH_2Cl_2–hexane) to yield **4** (2.85 g, 83%). M.p. 398 °C (DSC); ν_{max}(film)/cm^{-1} 3011, 1511, 1434, 1311, 1173, 860, 799 cm^{-1}; ^{1}H NMR ($CDCl_3$, 400 MHz) δ 7.32 (2H, s, Ar–H), 7.11 (8H, d, *J* 8.0, Ar–H), 7.08 (8H, d, *J* 8.0, Ar–H), 6.97 (2H, s, Ar–H), 2.33 (12H, s, 4 × Ar–CH_3); ^{13}C NMR ($CDCl_3$, 100 MHz) δ 154.4, 152.2, 141.1, 140.9, 136.5, 134.8, 129.0, 127.6, 125.7, 117.0, 113.7, 63.3, 21.1; MS (*m*/*z*, FAB$^+$) 154.1 (100); HRMS Calcd for $C_{44}H_{32}{}^{79}Br_2S_2$ 782.0312, found 782.0325; HRMS Calcd for $C_{44}H_{32}{}^{79}Br^{81}BrS_2$ 784.0292, found 784.0330; HRMS Calcd for $C_{44}H_{32}{}^{81}Br_2S_2$ 786.0271, found 786.0272.

Synthesis of DPAInT2

$Pd(OAc)_2$ (56 mg, 0.25 mmol), $HNPh_2$ (1.10 g, 6.5 mmol), Na*t*-BuO (3.60 mg, 37.5 mmol), and **4** (1.96 g, 2.5 mmol) were placed in a 250 mL two-neck flask equipped with a septum. The flask was evacuated and back-filled with argon. Toluene (50 mL) and *t*Bu_3P (0.05 M in toluene, 10 mL, 0.5 mmol) were added sequentially *via* syringe at room temperature. After heating at 110 °C for 48 h, the reaction mixture was cooled to room temperature and quenched with water (80 mL). The mixture was extracted with CH_2Cl_2 (3 × 80 mL). The combined organic phases were dried ($MgSO_4$) and concentrated *in vacuo* to yield **DPAInT2** (2.20 g, 91%), which was purified through recrystallization (CH_2Cl_2–hexane). M.p. 423 °C (DSC); ν_{max}(film)/cm^{-1} 1593, 1475, 1398, 1239, 758, 697 cm^{-1}; ^{1}H NMR (CD_2Cl_2, 400 MHz) δ 7.20–7.16 (12H, m, Ar–H), 7.07–7.05 (10H, m, Ar–H), 7.02 (8H, d, *J* 8.4,), 6.97 (10H, d, *J* 8.4, Ar–H), 2.23 (12H, s, 4 × Ar–CH_3); ^{13}C NMR (CD_2Cl_2, 400 MHz) δ 125.4, 124.9, 124.6, 124.4, 124.1, 123.1, 119.1, 16.4; MS (*m*/*z*, FAB$^+$) 960 (5); HRMS Calcd for $C_{68}H_{52}N_2S_2$ 960.3572, found 960.3552; Anal. Calcd for $C_{68}H_{52}N_2S_2$ C, 84.96; H, 5.45; N, 2.91; found C, 84.75; H, 5.46; N, 2.82.

Synthesis of dibromide 6

A solution of Br_2 (1.41 g, 8.8 mmol, 2.2 eq.) in $CHCl_3$ (15 mL) was added dropwise to a stirred solution of **5** (2.46 g, 4 mmol, 1 eq.) and $FeCl_3$ (32 mg, 0.2 mmol, 0.05 eq.) in $CHCl_3$ (15 mL) at 0 °C. After stirring for 5 h, the solution was quenched with 2 M K_2CO_3 (20 mL). The mixture was extracted twice with $CHCl_3$. The combined organic phases were washed with brine, dried ($MgSO_4$), and then concentrated through rotary evaporation. After washing with hexane, the product was obtained as a white solid (2.74 g, 95%). M.p. >400 °C; ν_{max}(film)/cm^{-1} ν 3054, 2987, 1422, 1265, 896, 742, 705 cm^{-1}; ^{1}H NMR ($CDCl_3$, 400 MHz) δ 7.67(2H, s, Ar–H), 7.50–7.47 (4H, m, Ar–H) 7.42 (2H, dd, *J* 1.6 and 8.4, Ar–H), 7.11 (8H, d, *J* 8.4, Ar–H), 7.07 (8H, d, *J* 8.4, Ar–H), 3.33 (12H, s, 4 × Ar–CH_3); ^{13}C NMR ($CDCl_3$, 100 MHz) δ 153.6, 151.1, 142.1, 139.2, 138.7, 136.4, 130.4, 129.1, 129.0, 127.9, 121.4, 121.2, 117.6, 64.6, 21.1; MS (*m*/*z*, FAB$^+$) 774 (3.3); HRMS (*m*/*z*, FAB$^+$) Calcd for $C_{48}H_{36}{}^{81}Br_2$ 774.1143, found 774.1177; Calcd for $C_{48}H_{36}{}^{81}Br^{79}Br$ 772.1163, found 772.1196; Calcd for $C_{48}H_{36}{}^{79}Br_2$ 770.1184, found 770.1157.

Synthesis of DPAInF

A mixture of **6** (1.55 g, 2 mmol, 1 eq.), diphenylamine (1.69 g, 10 mmol, 5 eq.), $Pd(OAc)_2$ (22.4 mg, 0.1 mmol), NaO*t*Bu (1.15 g,

12 mmol, 6 eq.), tBu$_3$P (0.05 M in toluene, 4 mL, 0.15 mmol), and toluene (30 mL) was heated under reflux for 2 d. After cooling to room temperature, the mixture was extracted twice with CH_2Cl_2. The combined organic phases were washed with brine and dried ($MgSO_4$); the product was isolated as while crystals after recrystallization (CH_2Cl_2–hexanes, 1 : 1) to afford **DPAInF** (1.29 g, 68%). M.p. 390–391 °C (DSC); ν_{max}(film)/cm^{-1} ν 3054, 2987, 1422, 1266, 896, 735, 705 cm^{-1}; ^{1}H NMR ($CDCl_3$, 400 MHz) δ 7.58 (2H, s, Ar–H), 7.46 (2H, d, J 8.8, Ar–H) 7.20–7.17 (10H, m, Ar–H), 7.09 (8H, d, J 8.0, Ar–H), 7.04–6.94 (22H, m, Ar–H) 2.31 (12H, s, 4 × Ar–CH_3); ^{13}C NMR ($C_2D_2Cl_4$, 100 MHz) δ 152.4, 150.1, 146.6, 146.4, 142.1, 138.1, 135.5, 133.9, 128.6, 128.3, 127.6, 123.4, 122.6, 122.2, 121.2, 119.8, 116.7, 64.2, 21.3; MS (m/z, FAB) 949 (0.3); HRMS (m/z, FAB$^+$) Calcd for $C_{72}H_{56}N_2$ 948.4443, found 948.4444; Anal. Calcd. C, 91.10; H, 5.95; N, 2.95. Found C, 90.93; H, 6.08; N, 2.64.

Cyclic voltammetry

The oxidation potentials were determined by cyclic voltammetry (CV) in CH_2Cl_2 solution (1.0 mM) containing 0.1 M tetra-n-butylammonium hexafluorophosphate ($TBAPF_6$) as a supporting electrolyte at a scan rate of 100 mV s^{-1}. The reduction potentials were determined by CV in THF solution (1.0 mM) containing 0.1 M tetra-n-butylammonium perchlorate (TBAP). A glassy carbon electrode and a platinum wire were used as the working and counter electrodes, respectively. The ferrocene/ferrocenium redox couples occur at values of E_o' of +0.61 V in THF/TBAP and +0.45 V in CH_2Cl_2/$TBAPF_6$, respectively, *vs.* Ag/AgCl (saturated). All potentials were recorded *versus* Ag/AgCl (saturated) as a reference electrode.

Photophysical properties measurements

Steady state spectroscopic measurements were conducted both in solution (1.0 × 10^{-6} M in dichloromethane) and solid films prepared by vacuum (2 × 10^{-6} torr) deposition on a quartz plate (1.6 × 1.0 cm). Absorption spectra were recorded with a U2800A spectrophotometer (Hitachi) and fluorescence spectra were acquired on a F4500 fluorescence spectrophotometer (Hitachi) upon exciting at the absorption maxima (416 nm for solution; 422 nm for solid film). Quantum efficiency measurements were recorded with an integration sphere coupled with a photonic multi-channel analyzer C10027 (Hamamatsu), which gave anthracene a quantum yield of 23%.

Ultraviolet photoemission spectroscopy (UPS) measurement

The valence-band ultraviolet photoemission spectra were carried out with He I (21.2 eV) and He II (40.8 eV) as excitation sources. The Fermi level of the system was measured on the gold substrate before the organic deposition. The energy levels of the HOMOs of organic samples were determined by extrapolating the edges of the HOMO peak down to the background of the UPS spectra. The vacuum levels of the films were deduced from the onset of lowest binding energy in the spectra and the photon energy of excitation sources.

Time-of-flight (TOF) mobility measurements

The samples for the TOF measurement were prepared by vacuum deposition using the structure: glass/Ag(30 nm)/ organic (2–3 μm)/Al(150 nm), and then placed inside a cryostat and kept under vacuum. All organic materials were purified by train sublimation before use. The thicknesses of the organic films were monitored *in situ* with a quartz crystal sensor and calibrated by a profilometer (Tencor Alpha-step 500). A pulsed nitrogen tunable dye laser was used as the excitation light source (to match the absorption of organic films) through the semitransparent electrode (Ag) induced photogeneration of a thin sheet of excess carriers. Under an applied dc bias, the transient photocurrent was swept across the bulk of the organic film toward the collection electrode (Al), and then recorded with a digital storage oscilloscope. Depending on the polarity of the applied bias, selected carriers (holes or electrons) are swept across the sample with a transit time of t_T. With the applied bias V and the sample thickness D, the applied electric field E is V/D, and the carrier mobility is then given by $\mu = D/(t_T E) = D^2/(Vt_T)$, in which the carrier transit time, t_T, can be extracted from the intersection point of two asymptotes to the plateau and the tail sections in double-logarithmic plots.

OLED device fabrications

ITO substrates were cleaned in an ultrasonic detergent bath, followed by acetone and methanol. The substrates were subsequently treated in an UV-ozone cleaner to remove any residual organic contaminants. A hole-injection layer of poly(3,4-ethylenedioxythiophene)-poly(4-stylenesurfonate) (PEDOT:PSS) was spin coated first onto the ITO substrate followed by drying at 120 °C for 30 min to remove residual solvent. Organic layers were then vacuum deposited at a deposition rate of 2–3 Å s^{-1}. Finally, 0.5 nm of LiF and a 100 nm thick Al cathode were deposited through a shadow mask with an area of 0.10 cm^2. OLED device characterization was carried out with a computer-controlled Keithley 6430 source meter and Keithley 6487 picoammeter equipped with a calibrated silicon photodetector at 25 °C under nitrogen atmosphere. EL spectra were measured using a photodiode array (Ocean Optics S2000) with a spectral range from 200 to 850 nm and a resolution of 2 nm.

Acknowledgements

This study was supported financially by the National Science Council and the Ministry of Economic Affairs of Taiwan.

References

1 C. W. Tang and S. A. Van Slyke, *Appl. Phys. Lett.*, 1987, **51**, 913.
2 (*a*) K. Yamashita, J. Futenma, T. Mori and T. Mizutani, *Synth. Met.*, 2000, **87**, 111; (*b*) C. H. Chen and C. W. Tang, *Appl. Phys. Lett.*, 2001, **79**, 3711; (*c*) M.-T. Lee, C.-K. Yen, W.-P. Yang, H.-H. Chen, C.-H. Liao, C.-H. Tsai and C.-H. Chen, *Org. Lett.*, 2004, **6**, 1241.
3 S. E. Shaheen, B. Kippelen, N. Peyghambarian, J. F. Wang, J. D. Anderson, E. A. Mash, P. A. Lee, N. R. Armstrong and Y. Kawable, *J. Appl. Phys.*, 1999, **85**, 7939.
4 Y. T. Tao, E. Balasubramaniam, A. Danel, B. Jarosz and P. Tomasik, *Appl. Phys. Lett.*, 2000, **77**, 1575.
5 (*a*) X. Xu, G. Yu, S. Chen, C. Di and Y. J. Liu, *J. Mater. Chem.*, 2008, **18**, 299; (*b*) K. R. J. Thomas, J.-T. Lin, Y.-T. Tao and C.-H. Chuen, *Chem. Mater.*, 2002, **14**, 2796.

6 (*a*) C.-W. Ko, Y.-T. Tao, J. T. Lin and K. R. J. Thomas, *Chem. Mater.*, 2002, **14**, 357; (*b*) K. R. J. Thomas, M. Velusamy, J.-T. Lin, Y.-T. Tao and C.-H. Chuen, *Adv. Funct. Mater.*, 2004, **14**, 387; (*c*) H. Choukri, A. Fischer, S. Forget, S. Chenais, M.-C. Castex, B. Geffroy, D. Ades and A. Siove, *Synth. Met.*, 2007, **157**, 198; (*d*) Y. Liu, C.-A. Di, Y. Xin, G. Yu, Y. Liu, Q. He, F. Bai, S. Xu and S. Cao, *Synth. Met.*, 2006, **156**, 824; (*e*) Y. Xing, X. Xu, P. Zhang, W. Tian, G. Yu, P. Lu, Y. Liu and D. Zhu, *Chem. Phys. Lett.*, 2005, **408**, 169.
7 M. A. Baldo, D. F. O'Brien, Y. You, A. Shoustikov, S. Sibley, M. E. Thompson and S. R. Forrest, *Nature*, 1998, **395**, 151.
8 A. Saitoh, N. Yamada, M. Yashima, K. Okinaka, A. Senoo, K. Ueno, D. Tanaka and R. Yashiro, *SID Int. Symp. Digest Tech.*, 2004, **35**, 150.
9 H. Antoniadis, M. Inbasekaran, E. Woo and P., *Appl. Phys. Lett.*, 1998, **73**, 3055.
10 (*a*) Q.-X. Tong, S.-L. Lai, M.-Y. Chan, Y.-C. Zhou, H.-L. Kwong, C.-S. Lee and S.-T. Lee, *Chem. Phys. Lett.*, 2008, **455**, 79; (*b*) Q.-X. Tong, S.-L. Lai, M.-Y. Chan, K.-H. Lai, J.-X. Tang, H.-L. Kwong, C.-S. Lee and S.-T. Lee, *Appl. Phys. Lett.*, 2007, **91**, 153504.
11 (*a*) A. Kraft, C. A. Grimsdale and B. A. Homes, *Angew. Chem., Int. Ed.*, 1998, **37**, 402; (*b*) K. R. Justin, J. T. Lin, M. Velusamy, Y.-T. Tao and C.-H. Chuen, *Adv. Funct. Mater.*, 2004, **14**, 83; (*c*) M. Akhtaruzzaman, M. Tomura, M. B. Zaman, J. Nishida and Y. Yamashita, *J. Org. Chem.*, 2002, **67**, 7813; (*d*) J. M. Raimundo, P. Blanchard, H. Brisset, S. Akoudad and J. Roncali, *Chem. Commun.*, 2000, 939; (*e*) B. A. D. Neto, A. S. Lopes, G. Ebeling, R. S. Gonçalves, V. E. U. Costa, F. H. Quina and J. Dupont, *Tetrahedron*, 2005, **61**, 10975.
12 T.-C. Chao, Y.-T. Lin, C.-Y. Yang, T. S. Hung, H.-C. Chou, C.-C. Wu and K.-T. Wong, *Adv. Mater.*, 2005, **17**, 992.
13 (*a*) U. Bach, K. D. Cloedt, H. Spreitzer and M. Grätzel, *Adv. Mater.*, 2000, **12**, 1060; (*b*) K.-T. Wong, Z.-J. Wang, Y.-Y. Chien and C.-L. Wang, *Org. Lett.*, 2001, **3**, 2285; (*c*) R. D. Hreha, C. P. George, A. Haldi, B. Domercq, M. Malagoli, S. Barlow, J.-L. Brédas, B. Kippelen and S. R. Marder, *Adv. Funct. Mater.*, 2003, **13**, 967; (*d*) Y.-L. Liao, W.-Y. Hung, T.-H. Hou, C.-Y. Lin and K.-T. Wong, *Chem. Mater.*, 2007, **19**, 6350.
14 (*a*) K.-T. Wong, L.-C. Chi, S.-C. Huang, Y.-L. Liao, Y.-H. Liu and Y. Wang, *Org. Lett.*, 2006, **8**, 5029; (*b*) K.-T. Wong, T.-C. Chao, L.-C. Chi, Y.-Y. Chu, A. Balaiah, S.-F. Chiu, Y.-H. Liu and Y. Wang, *Org. Lett.*, 2006, **8**, 5033; (*c*) H. Ebata, E. Miyazaki, T. Yamamoto and K. Takimiya, *Org. Lett.*, 2007, **9**, 4499; (*d*) Y. Wu, J. Zhang and Z. Bo, *Org. Lett.*, 2007, **9**, 4435; (*e*) C. Poriel, J. Rault-Berthelot, F. Barriere and A. M. Z. Slawin, *Org. Lett.*, 2008, **10**, 373.
15 Y. Kawamura, H. Sasabe and C. Adachi, *Jpn. J. Appl. Phys., Part 1*, 2004, **43**, 7729.
16 (*a*) H. Mattoussi, H. Murata, C. D. Merritt, Y. Iizumi, J. Kido and A. H. Kafafi, *J. Appl. Phys.*, 1999, **86**, 2642; (*b*) D. Z. Garbuzov, S. R. Forrest, A. G. Tsekoun, V. Bulovic and M. E. Thompson, *J. Appl. Phys.*, 1996, **80**, 4644.
17 (*a*) P. M. Borsenberger and D. S. Weiss, *Organic Photoreceptors for Imaging Systems*, Marcel Dekker, New York, 1993; (*b*) Y.-L. Liao, C.-Y. Lin, K.-T. Wong, W.-Y. Hung and W.-J. Chen, *Chem. Commun.*, 2007, 1831.
18 (*a*) M. P. de Jong, L. J. van Ijzendoorn and M. J. A. de Voigt, *Appl. Phys. Lett.*, 2000, **77**, 2255; (*b*) K. W. Wong, H. L. Yip, Y. Luo, K. Y. Wong, W. M. Lau, K. H. Low, H. F. Chow, Z. Q. Gao, W. L. Yeung and C. C. Chang, *Appl. Phys. Lett.*, 2002, **80**, 2788.

